

## Further evidence of spinodal decomposition during the induction period of polymer crystallization: Time-resolved small-angle x-ray scattering prior to crystallization of poly(ethylene naphthalate)

G. Matsuba, T. Kanaya, M. Saito, K. Kaji, and K. Nishida

*Institute for Chemical Research, Kyoto University, Gokasho, Uji, Kyoto-fu 611-0011, Japan*

(Received 19 April 2000)

Aiming to clarify spinodal decomposition of polymers in the induction period of crystallization, time-resolved small-angle x-ray scattering measurements have been made *in situ* for poly(ethylene naphthalate) while it was crystallized from the glass, or in the case of the so-called glass crystallization. It is confirmed for this polymer that in the very beginning of the induction period a scattering peak appears at around  $0.03 \text{ \AA}^{-1}$  in scattering vector  $q$ , which corresponds to a characteristic wavelength of  $200 \text{ \AA}$  in density fluctuations, and grows with time. Time evolution of this scattering peak is described by the kinetics of the spinodal decomposition as previously reported for the glass crystallization of poly(ethylene terephthalate).

PACS number(s): 61.41.+e, 61.10.Eq, 68.75.+x

In recent years, the structure formation of polymers in the induction period prior to crystal nucleation has received much attention. Imai and co-workers discovered a surprising phenomenon for the first time that a spinodal decomposition type of density fluctuations, whose characteristic wavelength is longer than the so-called long period, actually occurs during the induction period of crystallization [1,2]. This new finding was made by a small-angle x-ray scattering (SAXS) technique for the case of poly(ethylene terephthalate) (PET), which was crystallized from the glass just above the glass transition temperature,  $T_g$ . Such a spinodal decomposition can be understood based on the kinetic theory for the isotropic-to-nematic transition of polymer liquid crystals by Doi and co-workers [3–6]; it is caused by parallel orientational ordering of polymer rigid segments. Subsequently, Ezquerro *et al.* reported a similar result for the glass crystallization of poly(ether ketone ketone) (PEKK) by means of simultaneous real time wide-angle x-ray scattering (WAXS), SAXS, and dielectric spectroscopic techniques [7].

Furthermore, we have also succeeded in showing that the spinodal decomposition is triggered by the extension of rigid segments having crystalline conformation, which is caused by the change of polymer chain segments from amorphous to crystalline conformation as temperature is lowered below the melt temperature  $T_m$ . Such experiments were carried out for syndiotactic polystyrene (SPS) [8] and isotactic polystyrene (IPS) [9] using Fourier transform–infrared (FT-IR) spectroscopic and depolarized light scattering (DPLS) techniques. From a theoretical point of view, Olmsted *et al.* developed a completely new approach for the spinodal decomposition in polymer crystallization [10]. They constructed a phase diagram for polymer melts as functions of temperature and density, pointing out that two types of phase separation, binodal and spinodal, occur depending on the crystallization temperature.

The aim of this Rapid Communication is to confirm the generality of spinodal decomposition in the induction period. The density fluctuations in a glassy film of poly(ethylene naphthalate) (PEN) were *in situ* measured immediately after the temperature jump to a temperature above  $T_g$  using a

time-resolved SAXS technique. The PEN sample used for this experiment, which was supplied from Toyobo Co. Ltd., has a weight-average molecular weight  $M_w = 67\,000$  and a molecular distribution  $M_w/M_n = 2$ . An amorphous film about 1 mm thick was prepared by quenching a molten PEN film into ice-water after pressing for 3 min at a high temperature  $330 \text{ }^\circ\text{C}$  to remove the memory of the original samples. In order to remove the effect of water, the specimen was dried for 24 h under vacuum at room temperature. The melting temperature  $T_m$  and the glass transition temperature  $T_g$  of this sample were determined to be  $267 \text{ }^\circ\text{C}$  and  $110 \text{ }^\circ\text{C}$ , respectively, by differential scanning calorimetric (DSC) measurements at an increasing rate of  $5 \text{ }^\circ\text{C}/\text{min}$  using Perkin-Elmer DSC 7.

The melt-quenched samples were placed in a home-made temperature-controlled cell for SAXS measurements. After the temperature jump the time-resolved SAXS measurements were performed at a crystallization temperature ( $T_c = 155 \text{ }^\circ\text{C}$ ). For the SAXS measurements, we used the beam line BL-10C in a synchrotron radiation facility, Photon Factory at National Laboratory for High Energy Physics, Tsukuba, Japan. The storage ring was operated at an energy level of 1.7 GeV with a ring current 250 mA. The incident x-ray intensity of wavelength  $1.488 \text{ \AA}$  was monitored by an ionization chamber for the correction of a minor decrease of the primary beam intensity during the measurement. The scattering intensity was detected with a one-dimensional position sensitive proportional counter (PSPC) having 512 channels, and the camera length was about 2 m.

Figure 1 shows the crystallization isotherm  $\phi(t)$  of a melt-quenched PEN film at  $155 \text{ }^\circ\text{C}$  as a function of annealing time  $t$ , which was measured by DSC. During the first 25 min, neither exotherm nor endotherm is observed, indicating that the so-called induction period is 25 min. Note that we also confirmed from WAXS measurements that no Bragg peaks appear during the induction period.

Figure 2 shows time-resolved SAXS profiles in double logarithmic scales when the sample was annealed at  $155 \text{ }^\circ\text{C}$  as a function of the length of scattering vector,  $q$ ; for convenience each curve is shifted along the intensity axis. After 27

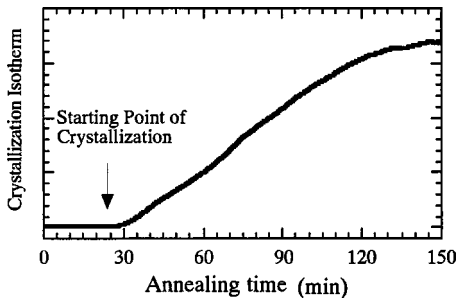


FIG. 1. Annealing time dependence of crystallization isotherm at 155 °C for PEN after the temperature jump from the glassy state. The induction period is estimated at 25 min.

min, a peak corresponding to the so-called long period appears near  $q=0.042 \text{ \AA}^{-1}$  (about 150 Å in spacing) and increases in intensity with time, while in the induction period a very broad peak does appear at about  $q=0.03 \text{ \AA}^{-1}$  and grows up slightly with annealing time, though it is rather hard to see in the logarithmic scales. This peak in the induction period is the same as the peak previously reported in the glass crystallization of PET by Imai and co-workers [1,2]. In order to analyze the scattering profiles in more detail, we subtracted the intensity of the melt-quenched sample from those of the annealed samples; the results are shown in Figs. 3 and 4. Figure 3 shows the resulting difference scattering intensity profiles in the induction period and just after crystal nucleation for the samples annealed for 2–32 min, showing that the scattering maximum clearly appears at around  $q = 0.03 \text{ \AA}^{-1}$  immediately after annealing at  $T_c = 155 \text{ °C}$ , although the data points are rather scattered during the induction period (25 min). As the annealing time increases, the maximum position shifts towards smaller  $q$  and the intensity increases. Figure 4 shows those for 32–120 min correspond-

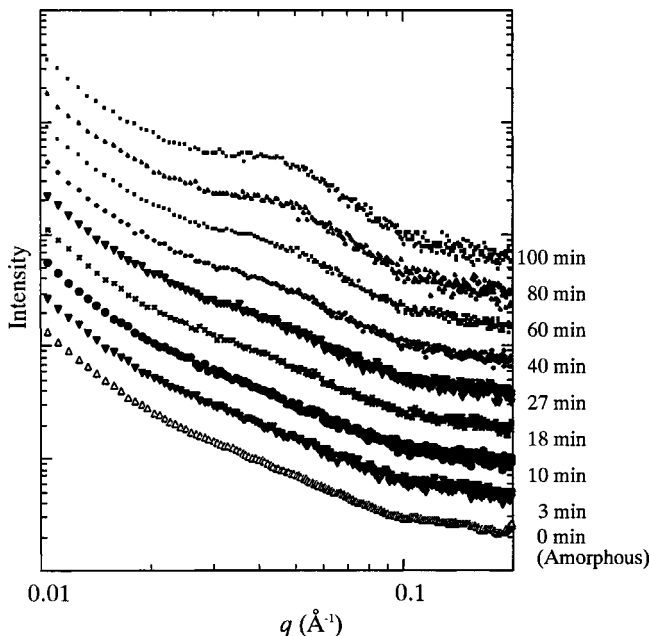


FIG. 2. Small angle x-ray scattering profiles of PEN as a function of annealing time for a melt-quenched glassy sample and samples annealed at 155 °C for 3, 10, 18, 27, 40, 60, 80, and 100 min. Each curve is shifted by a factor of 2.

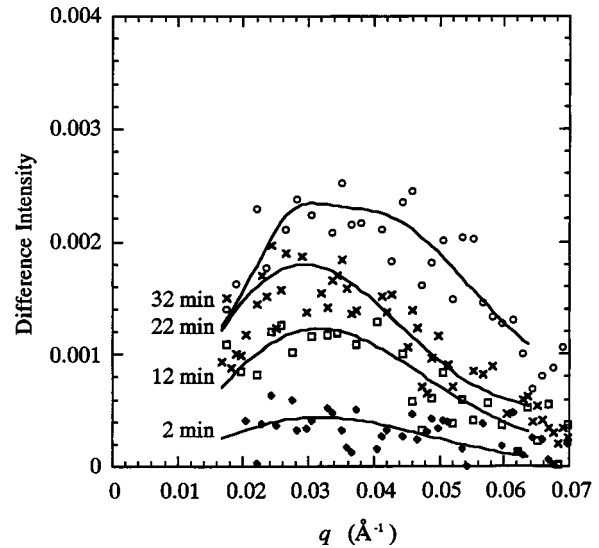


FIG. 3. Difference scattering intensity profiles of PEN during the induction period as a function of annealing time, when annealed at 155 °C for 2, 12, 22, and 32 min. The first three curves are within the induction period of 25 min.

ing to the crystallization stage, where the so-called long period peak appears at around  $q=0.04 \text{ \AA}^{-1}$ , and increases in intensity with annealing time. Even after the beginning of crystallization the peak at  $q=0.03 \text{ \AA}^{-1}$ , which appeared in the induction period, continues to grow, increasing in intensity and shifting gradually to lower  $q$  with annealing time. However, the peak at  $q=0.03 \text{ \AA}^{-1}$  is observed as only a shoulder of the long period peak at  $q=0.04 \text{ \AA}^{-1}$  in Fig. 4 because the peak does not shift largely compared with the case of PET and the intensities of the long period peak are much stronger than those of the peak at  $q=0.03 \text{ \AA}^{-1}$ .

The time evolution of the position and intensity of the peak appearing in a  $q$ -region smaller than the long period peak were analyzed in terms of the kinetics of the spinodal decomposition as in the case of PET previously reported [2]. First, we plot the maximum scattering intensity  $I_m$  and the

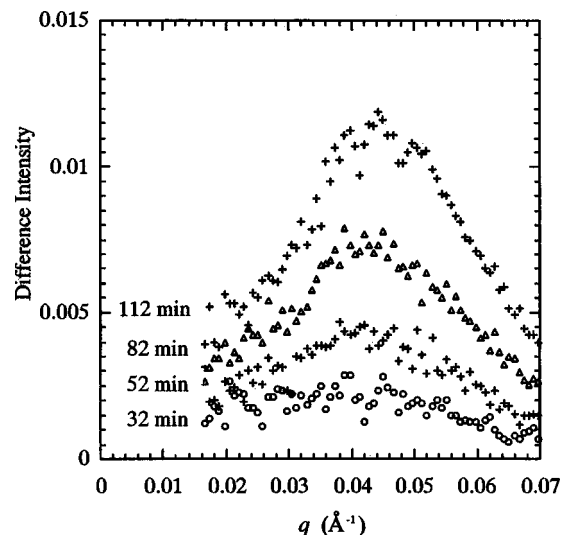


FIG. 4. Difference scattering intensity profiles of PEN in the crystallization stage as a function of annealing time when annealed at 155 °C for 32, 52, 82, and 112 min.

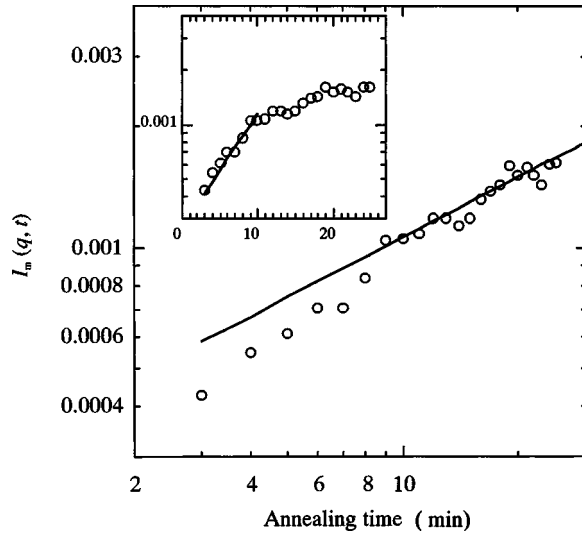


FIG. 5. Annealing time dependence of the maximum intensity  $I_m(q, t)$  during the induction period of crystallization. A solid line fitted with the observed points after 10 min shows  $I_m \sim t^{1/2}$ . A solid line before 10 min in the inset indicates  $I_m \sim \exp[R(q)t]$ .

scattering peak position  $q_m$  as a function of time during the induction period in Figs. 5 and 6, respectively. As seen from Fig. 5, before 10 min the maximum intensity  $I_m$  increases exponentially with annealing time, while the peak position is independent of annealing time as shown in Fig. 6. The features before 10 min agree with the prediction of a Cahn-Hilliard linearized theory [11,12] for the early stage of spinodal decomposition. According to this theory, the time evolution of scattering intensity  $I(q, t)$  is given by

$$I(q, t) = I_0 \exp[R(q)t], \quad (1)$$

where  $I_0$  is the initial scattered intensity and  $R(q)$  is the growth rate at a given  $q$ . This characteristic wavelength of density fluctuations is about  $200 \text{ \AA}$  and the maximum growth rate  $R(q_m)$  is about  $8.3 \times 10^{-4} \text{ s}^{-1}$ . This value of the maxi-

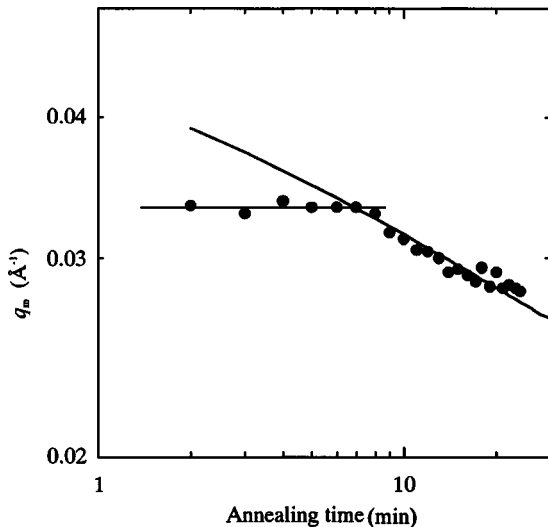


FIG. 6. Annealing time dependence of the peak position  $q_m$ . The two solid lines,  $q_m = 0.033 \text{ \AA}^{-1} (\sim t^0)$  and  $q_m \sim t^{-1/6}$ , corresponding to the early and late stages, respectively, are crosscovered at around 7 min.

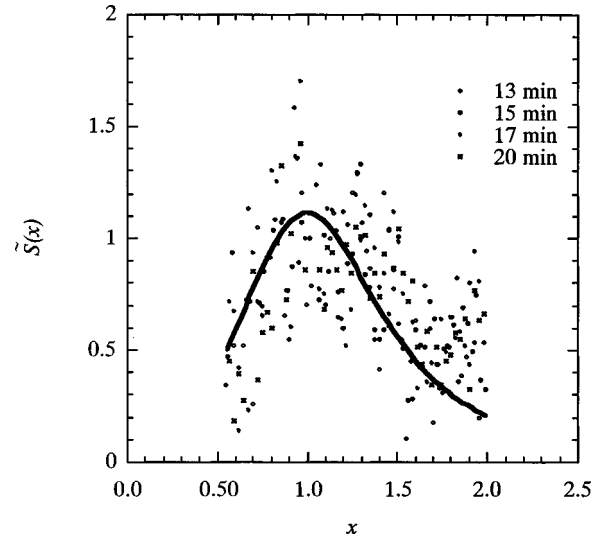


FIG. 7. Observed scaling structure function  $\tilde{S}(x)$  for the late stage calculated by Eq. (5) when the sample was annealed at  $155^\circ \text{C}$ . The solid curve indicates the theoretical  $\tilde{S}(x)$  of Eq. (4).

um growth rate of PEN is a little bigger than that of PET when crystallized at  $80^\circ \text{C}$  [2]. In the late stage of spinodal decomposition, it is well known that the amplitude of fluctuations reaches an equilibrium value and the characteristic size of the domain grows keeping a self-similarity. These characteristic features are explained by a Furukawa's dynamical scaling theory [13], which predicts that the peak position  $q_m$  and the maximum intensity  $I_m$  can be described using a single length parameter, cluster size  $R(t)$ ,

$$q_m \sim R^{-1}(t) \propto t^{-a}, \quad (2)$$

$$I_m \sim R^3(t) \propto t^b. \quad (3)$$

As seen from Fig. 6, the time dependence of  $q_m$  after 10 min obeys the power law of Eq. (2). Furthermore, the time dependence of the maximum intensity  $I_m$  can be also described by the power law of Eq. (3), as is shown in Fig. 5. The values of these exponents  $a$  and  $b$  are  $1/6$  and  $1/2$ , respectively. These values are in agreement with those estimated by Binder and Stauffer [14]. Naturally, the ratio  $b/a$  becomes the space dimension 3.0, being in good agreement with Furukawa's theory [13]. The universal scaling function  $\tilde{S}(x)$  in three dimensions is given by

$$\tilde{S}(x) = \frac{3x^2}{2+x^2}, \quad (4)$$

where  $x$  is defined as  $x = q[R(t)] = q/q_m(t)$ . The observed intensity  $I(q, t)$  is related to  $\tilde{S}(x)$  through

$$\tilde{S}(x) \sim \frac{S(q, t)}{R^3(t)} \sim q_m^3(t) I(q, t). \quad (5)$$

Figure 7 shows the observed  $q_m^3(t)I(q, t)$  and the theoretical scaling function  $\tilde{S}(x)$ . Although the observed data points are considerably scattered, Fig. 7 shows a tendency that the structure development in the late stage can be described by

the Furukawa's scaling theory [13]. These characteristic features in the late stage of PEN also coincide with those of PET crystallization.

In summary, when the amorphous PEN sample is annealed above  $T_g$ , a SAXS peak emerges at around  $0.03 \text{ \AA}^{-1}$  before crystal nucleation and grows with time. The growth process of this density fluctuation is described by the kinetics of a spinodal decomposition-type phase separation, as in the case of PET crystallization. In the early stage until 10 min the density fluctuations have a characteristic wavelength, 200  $\text{\AA}$ , independent of annealing time and the intensity of the peak increases exponentially with annealing time. These features can be described by the Cahn-Hilliard linearized theory [11,12]. In the late stage between 10 and 25 min the charac-

teristic wavelength of the density fluctuations and its intensity increase with annealing time obeying the power laws. These observations, as well as the evaluated values of exponents, agree well with the predictions of the Furukawa's scaling theory.

The experimental results obtained so far strongly support that the structure formation of PEN during the induction period of the glass crystallization can be well described by the kinetics of spinodal decomposition, similar to the case of the glass crystallization of PET.

We thank I. Fujio from Mitsui Chem. Co. Ltd. for the use of the high-power temperature controller and cell during the SAXS measurements in the Photon Factory at the National Laboratory for High Energy Physics, Tsukuba.

- 
- [1] M. Imai, K. Kaji, and T. Kanaya, *Phys. Rev. Lett.* **71**, 4162 (1993).
- [2] M. Imai, K. Mori, T. Mizukami, K. Kaji, and T. Kanaya, *Polymer* **33**, 4451 (1992).
- [3] M. Doi and S. F. Edwards, *The Theory of Polymer Physics* (Clarendon, Oxford, 1986).
- [4] T. Shimada, M. Doi, and K. Okano, *J. Chem. Phys.* **88**, 2815 (1988).
- [5] M. Doi, T. Shimada, and K. Okano, *J. Chem. Phys.* **88**, 4070 (1988).
- [6] T. Shimada, M. Doi, and K. Okano, *J. Chem. Phys.* **88**, 7181 (1988).
- [7] T. A. Ezquerro, E. López-Cabarcos, B. S. Hsiao, and F. J. Baltá-Calleja, *Phys. Rev. E* **54**, 989 (1996).
- [8] G. Matsuba, K. Kaji, K. Nishida, T. Kanaya, and M. Imai, *Macromolecules* **32**, 8932 (1999).
- [9] G. Matsuba, K. Kaji, K. Nishida, T. Kanaya, and M. Imai, *Polym. J. (Tokyo)* **31**, 722 (1988).
- [10] P. D. Olmsted, P. D. Poon, T. C. B. McLeish, N. J. Terrill, and A. J. Ryan, *Phys. Rev. Lett.* **81**, 373 (1988).
- [11] J. W. Cahn and J. E. Hilliard, *J. Chem. Phys.* **28**, 258 (1958).
- [12] J. W. Cahn, *J. Chem. Phys.* **42**, 93 (1965).
- [13] H. Furukawa, *Physica A* **123A**, 497 (1984).
- [14] K. Binder and D. Stauffer, *Phys. Rev. Lett.* **33**, 1006 (1974).